UCRL-JRNL-206551

Core Temperature and Density Profile Measurements In Inertial Confinement Fusion Implosions

J.A. Koch, N. Izumi, L.A. Welser, R.C. Mancini, S.W. Haan, T.W. Barbee, Jr., S. Dalhed, I.E. Golovkin, L. Klein, R.W. Lee, F.J. Marshall, D. Meyerhofer, H. Nishimura, Y. Ochi, and V. Smalyuk

This article was submitted to Physical Review Letters

08/25/2004

DISCLAIMER

Work performed under the auspices of the U.S. DOE by UC, LLNL contract No. W-7405-Eng-48.

Core Temperature and Density Profile Measurements in Inertial Confinement Fusion Implosions

J. A. Koch[1], N. Izumi[1], L. A. Welser[2], R. C. Mancini[2], S. W. Haan[1], T. W. Barbee[1], Jr., S. Dalhed[1], I. E. Golovkin[3], L. Klein[4], R. W. Lee[1], F. J. Marshall[5], D. Meyerhofer[5], H. Nishimura[6], Y. Ochi[6], T. C. Sangster[5], V. Smalyuk[5]

[1]*University of California, Lawrence Livermore National Laboratory, Livermore CA, USA*
[2]*Department of Physics, University of Nevada, Reno NV, USA*
[3]*Prism Computational Sciences, Madison WI, USA*
[4]*Department of Physics and Astronomy, Howard University, Washington DC, USA*
[5]*Laboratory for Laser Energetics, University of Rochester, Rochester NY, USA*
[6]*Institute of Laser Engineering, Osaka University, Japan*

Abstract

We have measured time-averaged electron temperature (T_e) and density (N_e) spatial profiles from indirect-drive implosions using an analytical analysis of multispectral x-ray imaging data. Measured T_e profiles are in good agreement with those predicted by one-dimensional hydrodynamics simulations, but measured and predicted N_e profiles are in significant disagreement. We conclude that mixing of shell material into the fuel can affect dopant emission-based measurements of core profiles even in relatively low-convergence implosions.

PACS Numbers: 52.25.Os, 52.57.Fg, 52.70.La

In inertial confinement fusion (ICF) experiments, high-power pulsed laser beams directly or indirectly ablate the outer surface of a spherical capsule containing hydrogen-isotope fuel [1]. The rocket effect compresses the capsule to an isobaric state, with maximum temperature and local-minimum density at the center of the plasma. Time-dependent temperature and density spatial profiles are determined by many factors, including laser drive symmetry, target symmetry, mixing of shell material into the fuel, and energy transport by electron and radiation conduction. Thermonuclear ignition in future ICF experiments will require precise tailoring of these profiles, and this Letter describes important progress in their measurement and interpretation.

X-ray imaging and spectroscopy have long been used to diagnose ICF plasmas, but these techniques have only recently been used to measure electron temperature (T_e) and density (N_e) profiles [2]. In those experiments, traces of argon were added to the fuel for spectroscopic diagnosis, and monochromatic x-ray images [3] at energies corresponding to the Ar He-β ($1s3p\text{-}1s^2$) transition were obtained along with x-ray spectra. A genetic algorithm-based two-objective search and reconstruction (SR) technique was then used to find the T_e and N_e profiles that yielded the best overall fit to both the Abel-inverted He-β image intensity profile and the space-integrated x-ray spectrum. However, because a single monochromatic image was available, reconstruction of T_e and N_e profiles relied on limited spatially-resolved data. The x-ray imaging approach also precluded the subtraction of background continuum emission images. Finally, spherical symmetry was assumed in the reconstruction process, and this introduces systematic errors in the T_e and N_e profiles unless the cores are highly spherical.

We have developed a new technique that allows direct analytical measurement of T_e and scaled N_e profiles and is free from the limitations described above. We

have used multiple-pinhole monochromatic imaging in the Ar He-β, Ar Ly-β (3p-1s), and nearby continuum energy bands, together with data analysis based on a generalized Abel inversion, to measure time-averaged Ar emissivity-weighted T_e and scaled N_e profiles from indirectly-driven ICF implosions for the first time. In our experiments, we used 30 500-joule, 1-ns-duration beams of the Omega laser [4] to irradiate the inside surface of a 2.5-mm-long, 1.6-mm-diameter Au hohlraum. The resulting x-ray drive imploded a 440-μm inner-diameter capsule, with a shell thickness of 35 μm, containing deuterium and argon gas with partial pressures of 50 and 0.1 atmospheres, respectively.

We viewed the implosion through a diagnostic hole from a direction nearly orthogonal to the hohlraum axis using a multiple-pinhole x-ray imager. This instrument consists of an array of 5-μm-diameter pinholes in a Ta substrate, a W/B_4C multilayer Bragg mirror with an interplanar spacing of 1.51 nm, and a time-integrated charge injection device (CID) x-ray detector. Each pinhole projects an 8X-magnified image of the implosion core onto the CID, and the Bragg reflection restricts the spectral content of the image. This imaging technique has been described elsewhere [5, 6]. The mirror provided a spectral range of 3 - 4.4 keV with a spectral resolution of ~ 0.5%.

Portions of many individual dark-field-subtracted pinhole images were added numerically using a centroid fitting analysis utilizing the symmetry properties of the pinhole array in order to improve signal-to-noise (S/N) ratio and to decouple spatial and spectral resolution. This analysis resulted in narrow-band (~ 60 eV-wide) images in three spectral windows: He-β, Ly-β and bremsstrahlung continuum between He-β and Ly-β. We then applied spectrally-dependent corrections to the relative image intensities due to filter transmission [7], CID sensitivity and quantum efficiency [8], and calculated mirror reflectivity, and we subtracted the nearby continuum images from the He-β and Ly-β line images.

The results were narrow-band images due to He-β, Ly-β and associated close satellite line emission only, relatively-calibrated for image intensity and averaged over dozens of individual pinhole images, with a calculated spatial resolution of 7 μm.

We next Abel-inverted [9] the image pixel maps row-by-row to obtain radial emissivity maps. In this step, we averaged the left and right sides of the image profile rows relative to their individual centroids. This process assumes only that each plane of the plasma perpendicular to the hohlraum axis has rotational symmetry about a line parallel to the hohlraum axis (along the columns of all images) with a center point that can vary with the longitudinal position of the plane; spherical or pure cylindrical symmetry need not be assumed. This process preserves much of the asymmetry of the original images. Neglecting opacity effects on the transport of the β lines (predicted optical depths are ~ 0.25), we obtained line emissivity maps for both energy bands as a function of local radius and longitudinal position along the hohlraum axis. In this step we masked the maps to discard all pixels where the local brightness divided by peak brightness in the original images fell below 10%; S/N ratio at this contrast level was typically 4:1.

Dividing the Ly-β emissivity map ε_L by the He-β emissivity map ε_H results in a map of local line emission ratio, and this ratio map was transformed to a local T_e map using tabulated $\varepsilon_L(T_e, N_e)$ and $\varepsilon_H(T_e, N_e)$ data generated by an atomic kinetics and radiation transport model [10]. The ratio $\varepsilon_L/\varepsilon_H$ is weakly dependent upon N_e ($\sim N_e^{-0.3}$ near $T_e = 1$ keV) and is therefore a well-defined function of T_e. We used the space-averaged Stark line widths of the β lines (obtained from the same data) to infer an emissivity-weighted average $N_e \approx 10^{24}$ cm^{-3}, and we used this single value of N_e to calculate the T_e profiles. The ε_L or ε_H maps were then combined with the T_e maps to obtain scaled N_e maps using

either of the known functions $\varepsilon_L(T_e, N_e)$ or $\varepsilon_H(T_e, N_e)$; N_e maps obtained using ε_L and ε_H maps were essentially identical. Absolute N_e maps cannot be obtained directly from our analysis because our data are not absolutely calibrated for photon counting, but the spatial variation of N_e can be obtained directly. Our ratio-based approach contains few approximations and differs from earlier approaches [2] in that we solve for the T_e and scaled N_e maps directly and analytically, rather than finding them with a constrained SR method. However, both approaches rely on the assumption that the local Ar number density follows N_e, and the breakdown of this assumption can affect the profiles inferred from both analyses, as will be discussed below.

Fig. 1 shows measured image profiles for the He-β and Ly-β bands from several experiments. We show here only profiles across the midplane of the hohlraum near the centers of the images; perpendicular profiles were similar except in extreme cases of laser pointing asymmetry, where the images were visibly prolate. Data are time-integrated except from shot 28608, where snapshot images were recorded onto a gated framing camera near the time of peak core emission. In Fig. 2 we show inferred T_e and scaled N_e profiles from the six time-integrated experiments, analyzed from the images in Fig. 1 using the ratio-based technique described above. The gated data from shot 28606 were too noisy to allow instantaneous T_e and N_e profiles to be inferred. For two of these experiments, we also show inferred T_e and scaled N_e profiles extracted from the data using a three-objective implementation of the SR technique discussed in Ref. 2. This independent analysis [11] shared only the raw image data with the analytical ratio-based analysis described above, and inferred T_e and N_e profiles based on self-consistent fits to the measured He-β and Ly-β emissivity profiles along with space-integrated x-ray spectra measured in the same experiments. The profiles inferred from this analysis for the two experiments examined are in good

agreement with the ratio-based analysis within shot-to-shot scatter, which is dominated by variations in core symmetry caused by laser and target variations. We performed a 1D hydrodynamics simulation using the Hydra code [12] to generate simulated image, T_e and scaled N_e profiles for comparison with the experimental data. The simulation used an experimentally-derived x-ray drive to implode a capsule having our experimental parameters, and calculated time-dependent T_e and N_e profiles in the absence of shell/gas mixing and drive asymmetry. We then post-processed these profiles by using the same atomic physics model [10] to generate both time-integrated and snapshot (time of peak central T_e) simulated image profiles in the 60-eV-wide He-β and Ly-β bands, including full frequency-dependent radiation transport and opacity, and smoothed them with our experimental imaging resolution function. The simulated image profiles can then be compared directly with the experimental time-integrated and snapshot image profiles.

We then masked the simulated images to show only points where the local image intensity was > 10% of the peak image intensity, resampled them to match our experimental pixel size, and generated T_e and scaled N_e profiles using the ratio analysis and the same processing steps and codes used to analyze the experimental data. The resulting post-processed simulated time-integrated T_e and scaled N_e profiles can be compared directly with the analyzed time-integrated experimental data, and the resulting post-processed simulated snapshot T_e and scaled N_e profiles can be compared directly with the original Hydra simulated profiles at the time of peak central T_e as a check on the reliability of the data analysis.

We find that the measured time-integrated and snapshot He-β image profiles in Fig. 1(a) are in poor agreement with Hydra-based predictions, and generally fall off more rapidly at larger radii than predicted. This discrepancy is particularly

evident in the snapshot images. The measured time-integrated and snapshot Ly-β image profiles in Fig. 1(b) are in better agreement but also fall off more rapidly at larger radii.

The shapes of the measured time-integrated T_e profiles in Fig. 2(a) are in good agreement with the Hydra prediction, though central temperatures are cooler by an average of ~ 7%. This is probably within the systematic error bars of the relative intensity calibrations applied to the raw image data. However, the measured time-integrated N_e profiles in Fig. 2(b) are in poor agreement with the predicted profile, and fall off at significantly smaller radii than predicted by the simulations. Finally, we find excellent agreement between the simulated snapshot T_e and scaled N_e profiles and the profiles obtained from simulated image ratio analysis (Fig. 2(a) and 2(b)), demonstrating the reliability of our analytical ratio-based analysis of multispectral image data. We note that adding noise to the simulated intensity profiles at a level consistent with the data introduces small variations in the T_e and N_e profiles that are well within shot-to-shot scatter, so that realistic noise levels do not affect any of our conclusions.

Our x-ray emission-based technique cannot measure density in the shell region ($R > 35$ μm) because the high-density shell temperatures are too low. The time-averaged N_e profiles are therefore measurements of Ar emissivity-weighted density within the central hot core of the plasma. The Hydra time-averaged emissivity-weighted N_e profile peaks near $R = 30$ μm, partly due to image processing limitations and the steep gradient in the predicted He-β image intensity at larger radii (note the slight roll-over in the post-processed snapshot Hydra profile in Fig. 2(b) compared with the Hydra predicted N_e profile at the same time), but principally because examination of simulated T_e and N_e profiles at different times shows that the emissivity weighting begins to favor earlier times for $R > 30$ μm. At those earlier times (~ 100 ps before the time of peak

compression), densities near R = 30 μm are lower but temperatures and therefore emissivities are higher. This time-integration effect unavoidably couples the T_e and N_e profiles, but together with the observed significant disagreement between measured and predicted snapshot image profiles in Fig. 1(a), the data support the conclusion that the 1D simulation does not capture all the relevant physics during times of interest, with regards to either N_e or local Ar concentration, prior to and near the time of peak compression.

The most likely explanation for the reasonable qualitative agreement between the measured and predicted T_e profiles and the poor agreement between the measured and predicted N_e profiles is the presence of undoped plastic mixed into the Ar-doped deuterium fuel. If we characterize local mixing by the relative number density ratio $\gamma = N_{CH}/N_D$, we find that the local line emissivity for both He-β and Ly-β is reduced by a factor ~ $1/(1+7\gamma)$. This factor cancels in the emissivity ratio $\varepsilon_L/\varepsilon_H$ used to calculate local temperature in our analysis, leaving the inferred T_e profile unaffected, but manifests itself as a decrease in the emissivity and inferred N_e profiles at larger radii where mixing is most pronounced.

If we use an *ad hoc* power-law model $\gamma(r) = (r/r_0)^\alpha$, we can multiply the simulated time-integrated emissivity profiles by $1/(1+7\gamma(r))$ and recalculate the inferred post-processed time-integrated N_e profile (from Fig. 2(b)) for various values of α and r_0. Figure 3 shows the results assuming r_0 = 41 μm for α = 8 and 4, and assuming r_0 = 32 μm for α = 4. We see that decreasing the values of α and r_0, effectively increasing the penetration of shell material, flattens the predicted time-integrated N_e profile and brings it into good agreement with the experimental measurements *without* affecting the predicted T_e profile that is already in good agreement with the data. Shot-to-shot differences between the experimental N_e profiles can then be interpreted as being caused by different

levels of mixing, due for example to shell roughness and laser beam pointing and energy variations. The image profile discrepancies noted in Fig. 1 could also be attributed to mixing effects, particularly if the core temperatures are cooler as suggested by the data in Fig. 2(a). Direct evidence for mixing in our experiments also exists in the form of H-like and He-like Ti line emission that is visible in spectra from shells that have Ti-doped inner mandrels, though the weakness of those data preclude quantitative analysis.

We note that we can integrate the mass of plastic mixed into the core for various values of α and r_0. Assuming the central core density is 10^{24} cm^{-3} we estimate from Fig. 3 that a mass equivalent to ~ 2 - 5 μm out of the initial 35 μm shell thickness has mixed into the outer regions of the core within the radius r_0. This mass is slightly larger than previous estimates obtained from higher-convergence direct-drive implosions using a different approach [13-15]. Here, however, we can begin to infer the radial distribution of this mass, a measurement which would be valuable for comparison to hydrodynamic mix models. Finally, we note that our results may have impact on some of the previously observed discrepancies between measured and calculated T_e and N_e profiles in direct-drive implosions [16], which also utilized doped-core emission image data [2], and that our conclusions support previous comparisons between experimentally measured indirect-drive primary neutron yields and 1D clean simulation predictions [17], where the inclusion of mix effects in the simulation improved the agreement with experimental data.

It is intriguing that our inferred density curves are qualitatively different from those found in low-convergence direct-drive implosions [2,16], where the N_e profiles were flatter and rose slightly with radius. The analysis of those data relied on 2-objective SR, and a preliminary analysis of some of our own data using the same technique [18] resulted in similar density curves. Based on the

verified and consistent ratio and 3-objective SR analyses presented here, we conclude that our earlier analysis [18] was misled by reliance on spatially-integrated spectra and a single image, but the question of whether or not this impacts the analysis of the earlier experiments [2,16] remains open. Since we infer a shell mix depth (2-5 μm) that is 4-10 times larger than that inferred in high-convergence direct-drive implosions [13], it is unlikely in any case that the earlier low-convergence direct-drive experiments are affected by mix, so we would expect N_e profiles similar to those that were presented. Additional direct-drive implosion data, including multiple line-emission images that allow an analytical ratio analysis and a 3-objective SR analysis, will be required to address this question.

In summary, we have measured time-averaged T_e and scaled N_e profiles from indirect-drive implosions for the first time using a new combination of experimental and analytical techniques. We find that the measured time-averaged T_e profiles are in good agreement with those predicted by post-processed 1D clean hydrodynamics simulations, but we find significant discrepancies between measured and predicted time-averaged emissivity-weighted N_e profiles. This discrepancy is probably due to the presence of hydrodynamic mixing effects which are not treated in the 1D clean model and which can affect dopant emission-based core profile measurements. Future theoretical mix modeling and experiments, particularly including time-resolved T_e and N_e profile measurements and high-energy backlit radiography [19], would be valuable for further research. This work was performed under the auspices of the U.S. Department of Energy by the University of California Lawrence Livermore National Laboratory under contract No. W-7405-ENG-48, and by the University of Nevada, Reno, under DOE NLUF Grant No. DE-FG03-03SF22696. Partial support was also provided by DoE HEDS Grant No. DE-

FG03-98DP00213 to Howard University. We gratefully acknowledge C. Damian, V. Glebov, B. Hammel, O. Landen, M. Marinak, S. Regan, V. Rekow, C. Sorce, J. Soures, R. Turner, R. Wallace and the staff at LLE for discussions and support.

References

[1] J. D. Lindl, *Inertial Confinement Fusion* (AIP Press, New York, 1998) and references therein.

[2] I. Golovkin *et al.*, Phys. Rev. Lett. **88**, 045002-1 (2002).

[3] I. Uschmann *et al.*, Appl. Opt. **39**, 5865 (2000).

[4] T. R. Boehly *et al.*, Opt. Commun. **133**, 495 (1997).

[5] B. Yaakobi, F. J. Marshall, D. K. Bradley, Appl. Opt. **37**, 8074 (1998).

[6] J. A. Koch et al., Proc. Inertial Fusion Sciences and Applications 2003, Monterey, CA, Sept. 7-12, 2003.

[7] B. L. Henke, E. M. Gullikson, J. C. Davis, Atomic Data and Nuclear Data Tables **54** (2), 181 (1993).

[8] F. J. Marshall *et al.*, Rev. Sci. Instrum. **72**, 713 (2001).

[9] K. Bockasten, J. Opt. Soc. Am. **51**, 943 (1961).

[10] I. Golovkin *et al.*, J. Quant. Spectrosc. Radiat. Transfer **65**, 273 (2000).

[11] L.A. Welser *et al.*, Rev. Sci. Instrum. **74**, 1951 (2003).

[12] M. Marinak *et al.*, Phys. Plasmas **3**, 2070 (1996).

[13] S. P. Regan *et al.*, Phys. Rev. Lett **89**, 085003-1 (2002).

[14] P. B. Radha *et al.*, Phys. Plasmas **9**, 2208 (2002).

[15] C. K. Li *et al.*, Phys. Rev. Lett **89**, 165002-1 (2002).

[16] Y. Ochi *et al.*, Rev. Sci. Instruments **74**, 1683 (2003).

[17] P. Amendt *et al.*, Phys. Rev. Lett. **89**, 165001-1 (2002).

[18] L. A. Welser et al., J. Quant. Spectrosc. Radiat. Transfer **81**, 487 (2003).

[19] P. A. Norreys *et al.*, Phys. Plasmas **11**, 2746 (2004).

Figure Captions

Figure 1: Measured (points) and simulated (lines) He-β (a) and Ly-β (b) image profiles. All profiles are normalized to unity at x = 0 and are time-integrated except where noted. Hydra snapshot profiles are predicted at the time of peak core T_e, approximately corresponding to the time where the gated data from shot 28608 were obtained.

Figure 2: Measured and simulated T_e (a) and scaled N_e (b) profiles. Ratio and search-analyzed profiles are based on analysis of image data, and are masked to show only data points where the image intensities are greater than 10% of the peak intensity for both image profiles. Curves are time-integrated except where noted, and N_e profiles are normalized to unity at R = 0. Hydra snapshot profiles are predicted at the time of peak core T_e, and ratio-analyzed Hydra profiles are inferred using a ratio analysis of simulated images, either time-integrated or snapshot.

Figure 3: Measured and simulated scaled time-integrated N_e profiles from Fig. 2(b), plotted against mix-model simulated scaled N_e profiles for several values of the parameters α and r_0 described in the text. The legend for the data points is the same as shown in Fig. 2.

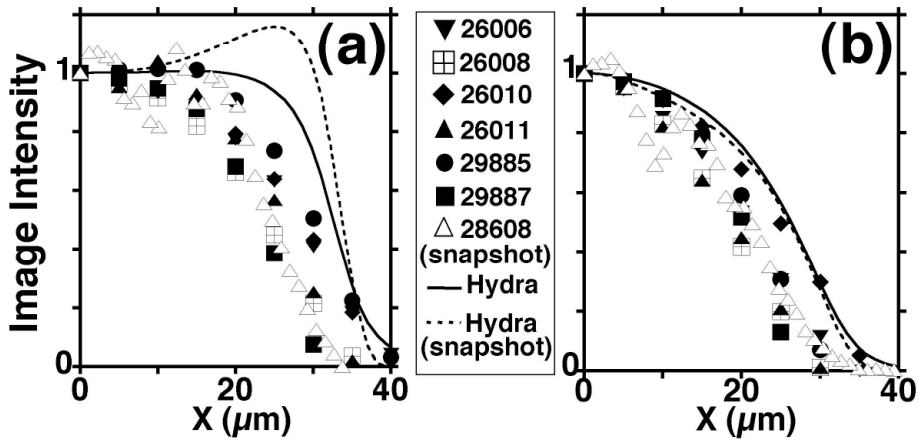

Figure 1: Koch et al., PRL

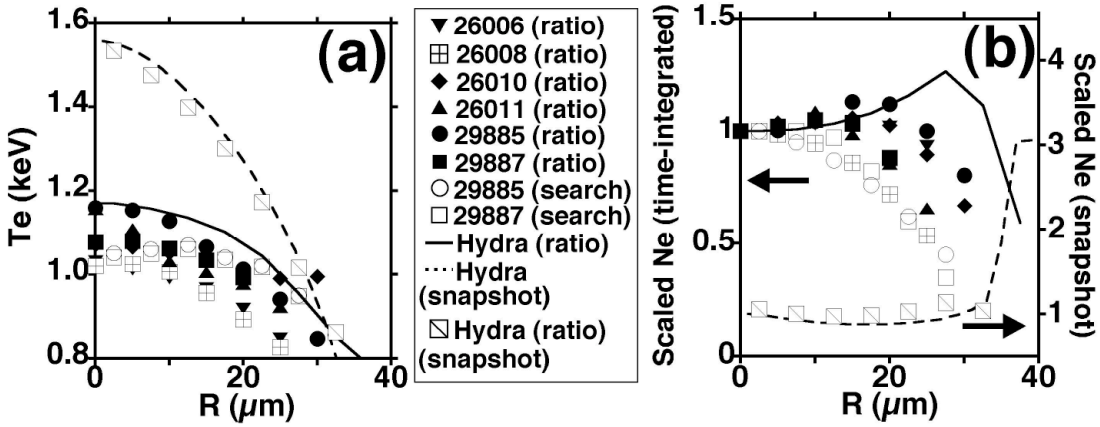

Figure 2: Koch et al., PRL

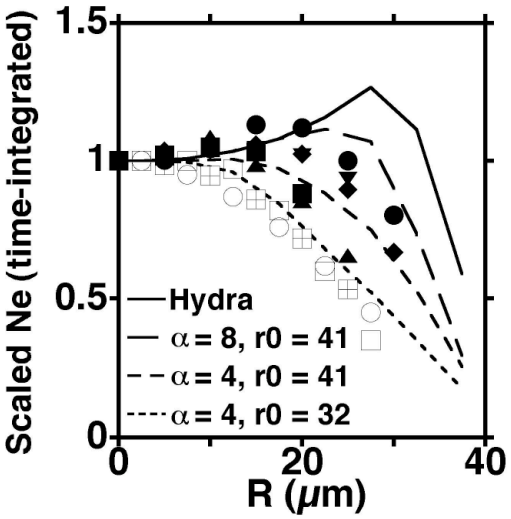

Figure 3: Koch et al., PRL